Construction and Building Materials 416 (2024) 135072

Contents lists available at ScienceDirect

Construction and Building Materials

journal homepage: www.elsevier.com/locate/conbuildmat

Influence of loading rate on bond shear strength of autoclaved aerated concrete masonry

Ningombam Reena Devi [a], Prateek Kumar Dhir [b,*], Pradip Sarkar [a]

[a] Department of Civil Engineering, National Institute of Technology Rourkela, 769008, India
[b] Department of Engineering, Durham University, Durham DH1 3LE, UK

ARTICLE INFO

Keywords:
Autoclaved aerated concrete (AAC)
Triplets
Shear strength
Loading rates
And pre-compression

ABSTRACT

This study aims to investigate the bond shear strength of autoclaved aerated concrete (AAC) masonry, focusing on the influence of pre-compression and load rates. Experimental results show that the bond shear strength of AAC masonry increases with increasing load rates as well as with increasing pre-compression stress. It is understood from the experimental studies that both loading rate and pre-compression stress significantly affect the failure mode and stress distribution of AAC masonry specimens under shear loading. To provide further insights, the paper aims to develop a nonlinear finite element modelling approach with Abaqus software employing detailed surface-based cohesive contact approaches, which can reliably capture the bond shear behaviour and failure modes of AAC masonry. Higher stress contours are seen at higher displacement rates due to the development of sudden dynamic and irregular loads compared to lower rates. The stress-strain characteristics and the deformed shape of the specimens obtained from the numerical analyses were found to be identical to those from the experimental studies. Instead of expensive and time-consuming experimental tests, the proposed numerical modelling approach can be an effective alternative to studying the bond shear behaviour of AAC masonry.

1. Introduction

Masonry was used widely as the predominant building material before concrete and steel were introduced in construction. Brick masonry is still the most popular building material, particularly in developing countries due to its easy handling and low costs in construction. Due to its many advantages, brick masonry is widely used for the construction of residential buildings (both load-bearing walls and infill walls of framed structures) that are exposed to various environmental conditions.

Masonry structures are an assemblage of brick-and-mortar units which are described as orthotropic, inelastic, and non-homogeneous. Shear strength is one of the most important mechanical parameters in the context of the estimation of the in-plane shear capacity of brick masonry. Again, shear failure is the dominant mode of failure observed in many masonry buildings subjected to lateral loads (such as earthquakes, strong winds, and floods), asymmetric vertical loads, support settlements, etc. The shear stress generally acts in combination with compression caused by the self-weight and floor loads. Confinement by, for instance, structural frames to infill walls may also lead to shear compression [1,2].

The present state of knowledge concerning shear strength and shear load-displacement behaviour of masonry is far less advanced than that concerning masonry behaviour in compression, even though shear failure is an important, often governing mode of failure in many masonry buildings [3]. Several studies [4–14] have shown the importance of shear strength of masonry in predicting true structural performance of the buildings. However, the lack of understanding is reflected by the low values of shear resistance allowed by present building codes [15,16].

Among all the available types of masonry used in the construction industry, autoclaved aerated concrete (AAC) block masonry is the most popular in many parts of the world due to its lightweight properties, good thermal and sound insulation properties, easy availability, good soundness, durability, and the low cost. However, an extensive literature review reveals that there are far fewer studies [17–23] on AAC block masonry compared to studies on traditional clay and fly ash brick masonry.

Studies [24–31] have demonstrated the importance of load rates in determining various mechanical properties of different building materials such as clay brick, concrete, geopolymer concrete, cement mortar, geopolymer mortar, polymer mortar, and cement asphalt mortar, and reported an increasing trend in shear strength when applied load rate

* Corresponding author.
E-mail address: prateek.dhir@strath.ac.uk (P.K. Dhir).

https://doi.org/10.1016/j.conbuildmat.2024.135072
Received 6 August 2023; Received in revised form 23 December 2023; Accepted 15 January 2024
Available online 31 January 2024

increases. However, all these studies were limited to the axial strength (tension and compression) behaviour of the materials.

Past literatures found that all the studies to evaluate the shear bond strength of AAC masonry have performed the shear strength test without considering pre-compression and load rates [32–36]. In order to take pre-compression into account when evaluating shear bond strength, masonry specimens must be loaded simultaneously in two directions, which requires the use of specialized testing equipment. The lack of such an apparatus may explain the lack of published literature on the shear strength of pre-compressed masonry. However, there are many previous literatures where the shear bond strength of clay brick masonry is reported considering pre-compression. Mojsilović [37] and Barattucci et al. [38] carried out an experimental study on the shear behaviour of clay brick masonry triplets subjected to monotonic and cyclic shear loads and concluded that the shear behaviour of the specimens was greatly influenced by the level of pre-compression applied. The peak shear strength observed during the monotonic and cyclic shear tests increased with increasing levels of pre-compression pressure. Hernoune et al. [39] presented an experimental and numerical study on retrofitted masonry triplets under shear load with different levels of pre-compression. This study reported that the shear strength increases with the increases in pre-compression. Therefore, the shear strength of masonry is a function of the pre-compression stress acting at the bed joint in addition to other factors such as the types of masonry unit and the mortar mix.

Numerical calculations of masonry structures based on the finite element method (FEM) are used at various construction stages starting from the design of modern brick buildings to the diagnostics of existing structures including the condition assessment of historic buildings [40]. Ferretti et al. [41] carried out experimental program on AAC masonry beams subjected to bending and masonry panels subjected to uniaxial and biaxial loads. The experimental results have been used for the calibration of the well-known macro-model proposed by Lourenço et al. [42,43] for the analysis of masonry structures. The effectiveness of the proposed model has been verified by simulating the experimental behaviour of a full-scale AAC masonry wall, through nonlinear finite element analysis. An experimental test program and numerical simulation was carried out by Hernoune et al. [39] to study the shear behaviour and the failure mechanism of brick masonry triplets under different levels of pre-compression. A detailed micro-modelling approach was taken in the Abaqus finite element software.

After a brief review of the literature, it is found that no study was found on the shear strength of AAC masonry considering pre-compression and loading rates. Therefore, the main objective of this study is identified as to investigate the shear strength properties of AAC block masonry considering pre-compressions under various loading rates. The evolution of finite element techniques allows for a more refined analysis of the structure these days. However, an extensive review of the literature indicates that there is limited information on the mechanical properties necessary for adequate mathematical modelling of brick masonry structures. Therefore, the last part of this article presents an attempt to study the numerical models of AAC block masonry with detailed distinctive brick-and-mortar modelling with their respective dynamic material properties obtained from laboratory tests. The failure pattern of the brick sample was also studied. The numerical implementation has been principally devoted to developing reliable interface models via adapted constitutive laws or incorporating fracture mechanics and plasticity theory concepts.

2. Research significance

Bed joint shear failure is the primary failure mode of brick masonry which is especially observed during natural events such as earthquakes. Pre-compression is one of the various crucial factors that significantly affect the shear strength of brick masonry. This paper presents for the first time the experimental results of the shear strength of AAC block masonry triplet specimens at different levels of pre-compression. The outcome of this paper will help to assess the shear capacity more accurately and thus help to better assess the safety of AAC block masonry structures.

This paper also presents the experimental results on the influence of loading rate on the shear behaviour of AAC block masonry for the first time. Masonry walls are likely to undergo very high loading rates during storm winds and earthquakes. Therefore, understanding the shear behaviour of AAC block masonry under different loading rates is of considerable importance.

To provide further insights into the behaviour, complementary nonlinear numerical simulations are undertaken, using the key parameters obtained from the laboratory experiments. The numerical models employ detailed surface-based cohesive-contact approaches, with due account for inelastic damage at the masonry interfaces, and damage-plasticity modelling for the constitutive response of brick materials. It is shown that the numerical approaches adopted can capture reliably the main behavioural characteristics and failure modes and can therefore be employed for further numerical assessments.

3. Experimental campaign

As discussed in the preceding section, the primary aim of the current study is to assess the impact of load rates and pre-compression on the shear-bond strength of AAC masonry assemblies. It is important to note that the strength characteristics of a masonry assembly are inherently linked to the properties of its constituent materials, including the AAC units and the mortar. Consequently, this section is dedicated to presenting the results of laboratory tests conducted on AAC units, ready-mix mortar, and ultimately, the AAC masonry triplets.

3.1. Tests on AAC units

Uniaxial compression test [44] and tensile test [17] were performed on a total of 36 AAC cube specimens of size 100 × 100 × 100 mm^3 (18 for compression test and 18 for tensile test) for three selected displacement rates (0.1, 1.0, and 10 mm/min). Additionally, the flexural strength of AAC masonry units was assessed through a three-point bending test [45] at three displacement rates (0.1, 1.0, and 10 mm/min), allowing for the indirect determination of uniaxial tensile strength. A total of 18 AAC beam specimens, measuring 40 mm × 40 mm × 160 mm, were tested for the flexural strength tests.

During the compression test, cracking at approximately 45° (as two truncated pyramids, with one overturned on the other) near the ends of the cubic specimens was noted (see Fig. 1a). The stress-strain relationships derived from the compression tests (shown in Fig. 2a) reveal that the peak stress, corresponding axial strain, and elastic modulus of the cubic AAC specimens exhibit an increasing trend with increasing displacement rate. The range of compressive strength and elastic modulus values observed in the experimentally evaluated AAC specimens aligns with findings from several prior studies [26,33,36]. For a more in-depth discussion on compressive strength, additional insights can be found in Devi et al. [23].

While the compressive strength stands out as the primary structural characteristic of the AAC masonry unit, it is noteworthy that the mechanical behavior is also impacted by its limited resistance to tensile stresses. The nominal splitting tensile strength (f_{st}) is determined based on the load at failure (P) using the elastic tensile stress theory (as per Eq. 1).

$$f_{st} = \frac{2P}{\pi A} \tag{1}$$

where A = area of the splitting surface.

Fig. 1b, illustrates the relationship between splitting tensile stress and axial strain for AAC cube specimens. The splitting tensile strength of

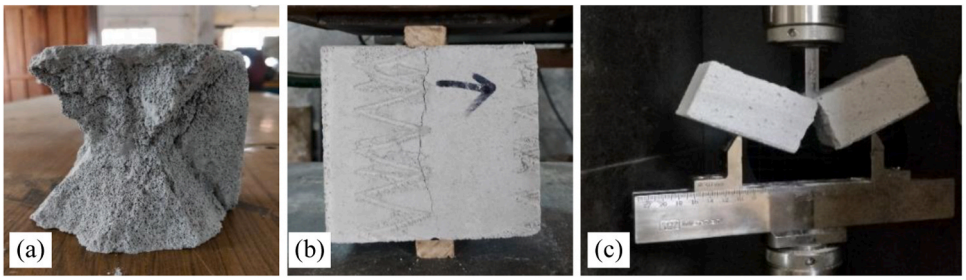

Fig. 1. (a) Uni-axial compression, (b) splitting tensile. and (c) three-point bending test of AAC block units.

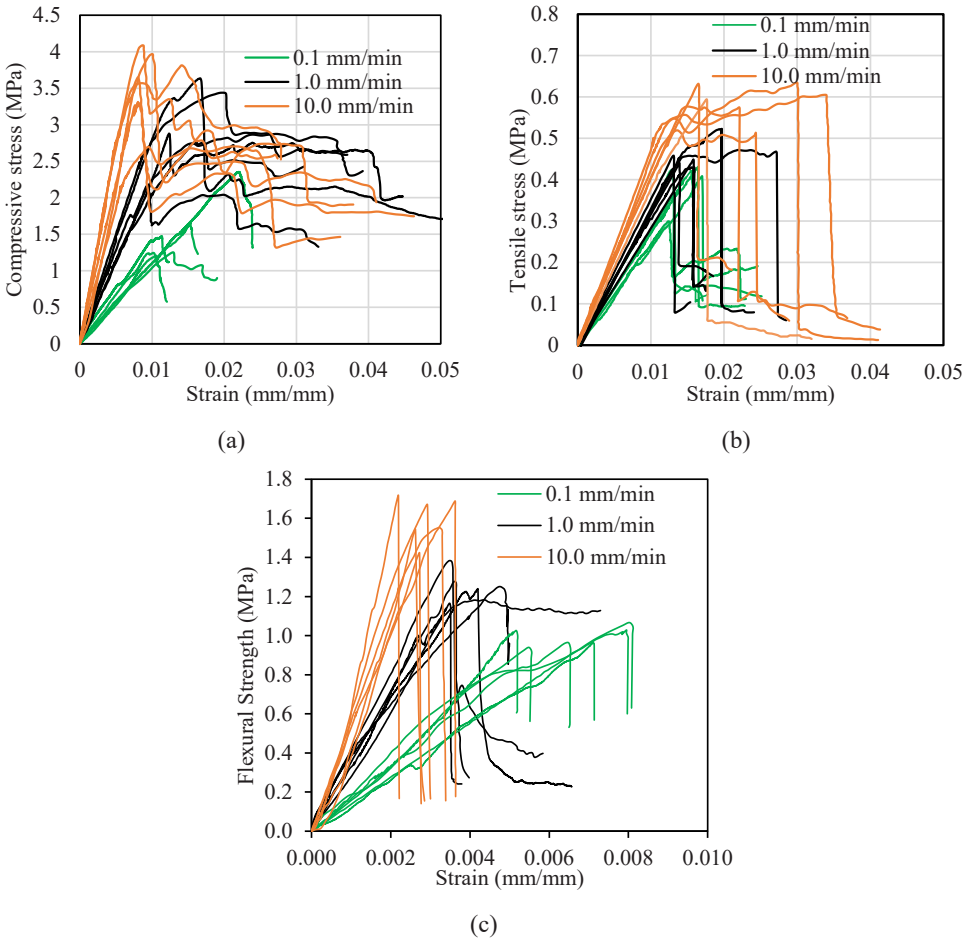

Fig. 2. Comparisons of (a) compressive, (b) tensile and (c) flexural strength of AAC block units.

these specimens increase with increasing displacement rate. Similar failure pattern is observed in the specimens tested for splitting tensile strength [17,46]. More discussions on the tensile strength of AAC units are available at Devi et. al. [23].

Similarly, the flexural strength of AAC beam specimens were evaluated using three-point bending test [45] at selected displacement rates from which the uniaxial tensile strength can be indirectly determined. Under a displacement-controlled universal testing machine the tests were performed, and the specimens were found to have experienced a brittle mode of failure at the peak load, with the development of a main crack placed near the mid-span as shown in Fig. 1b. Fig. 2b shows the load-displacement behaviours of the AAC blocks obtained at three different displacement rates. Generally, the load-displacement response is nearly linear up to failure load followed by a sudden drop in the post-peak zone. The results indicate that the displacement rate significantly influences the load-displacement behaviours of the AAC beam specimens.

Load-displacement curves obtained from the three-point bending test were used to calculate the mean flexural strength (R) and flexural modulus (E_{flex}). The flexural strength of the AAC beam specimen (R) was determined according to ASTM C1161–18 [45] as follows:

Table 1
Mean mechanical strength parameters of AAC block units.

Displacement rate (mm/min)	Compressive Strength (MPa)	Splitting Tensile Strength (MPa)	Flexural strength (MPa)
0.1	1.56 (0.26)	0.39 (0.12)	0.94 (0.18)
1.0	2.97 (0.16)	0.46 (0,06)	1.17 (0.16)
10.0	3.59 (0.13)	0.59 (0.07)	1.42 (0.13)

Note: the values in the parenthesis represent the coefficient of variation.

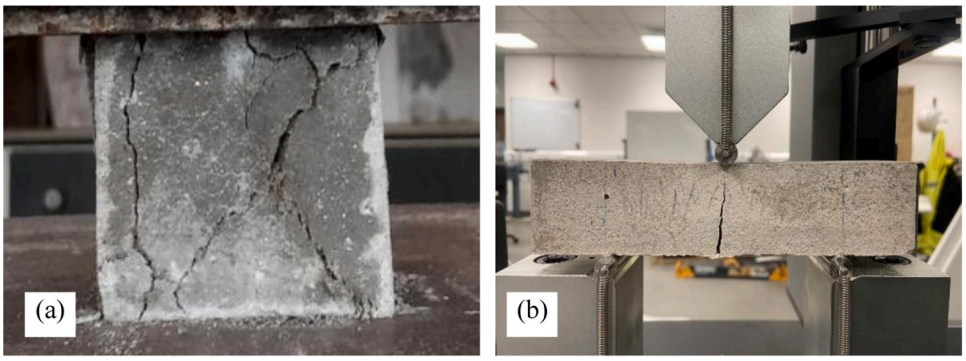

Fig. 3. (a) Compression test of mortar cubes, and (b) three-point bending test of mortar beams.

$$R = \frac{3PL}{2bd^2} \quad (2)$$

where P is the peak load, L is the span between the supports, b and d are the width and height of the vertical cross-section of the test specimen, respectively. The flexural strength (R) of all specimens is calculated using Eq. 2 and their mean values for different displacement rates are presented in Table 1. The flexural modulus (E_{flex}) of the AAC beam specimen is also calculated (Eq. 3) as per published literature [47,48], as follow:

$$E_{flex} = \frac{PL^3}{48\delta I} \quad (3)$$

where 'δ' represents the displacement at the peak load and 'I' represents the second moment of the cross-sectional area of the AAC beam specimen.

All mechanical strength properties of AAC at the selected displacement rates are presented in Table 1. The mean values of the splitting tensile strengths are in the typical range of 15–28% of the compressive strength. The compressive strength of AAC exhibits a 130% increase when the displacement rate is elevated from 0.1 mm/min to 10 mm/min. Likewise, the tensile and flexural strengths of AAC show a 50% increase with the rise in displacement rate from 0.1 mm/min to 10 mm/min.

Table 2
Mean mechanical strength properties of ready-mix mortar.

Displacement rate (mm/min)	Compressive strength (MPa)	Flexural strength (MPa)
0.1	4.86 (0.12)	1.67 (0.05)
1.0	8.41 (0.10)	2.16 (0.05)
10.0	10.64 (0.16)	3.27 (0.07)

Note: The values in the parenthesis represent coefficient of variation

3.2. Tests on mortar

Ready-mix block adhesive was used in the present study as the binder of the AAC masonry assemblage. To investigate the detailed strength parameters of the binder, the uniaxial compressive test and flexural strength test (3-pt bending) was performed in this study. 18 cube specimens of size 50 × 50 × 50 mm^3 (see Figs. 3a) and 18 beam specimens of size 40 × 40 × 160 mm^3 were tested (see Fig. 3b) for compressive strength [49] and flexural strength test [50] respectively.

In addition to the mortar cube compression test, mortar beam samples are also tested to characterise the flexural strength behaviour of the adhesive mortar. A three-point bending test was performed in a universal testing machine with a capacity of 30 kN at 0.1 mm/min, 1.0 mm/min and 10.0 mm/min.

Table 2 summarizes the mechanical strength parameters (compressive strength and flexural strength) of the tested mortar specimens. An increase in both compressive strength (Fig. 4a) and flexural strength (Fig. 4b) is observed with an increase in loading rate. A 119% and 96% increase observed for compressive and flexural strength respectively when the displacement rate increases from 0.1 mm/min to 10 mm/min.

3.3. Preparation and testing of AAC triplets

AAC blocks of size 600 × 200 × 100 mm^3 were collected from their respective batch to avoid variations derived from a change in their physical properties. The published literature, codes, and standards have

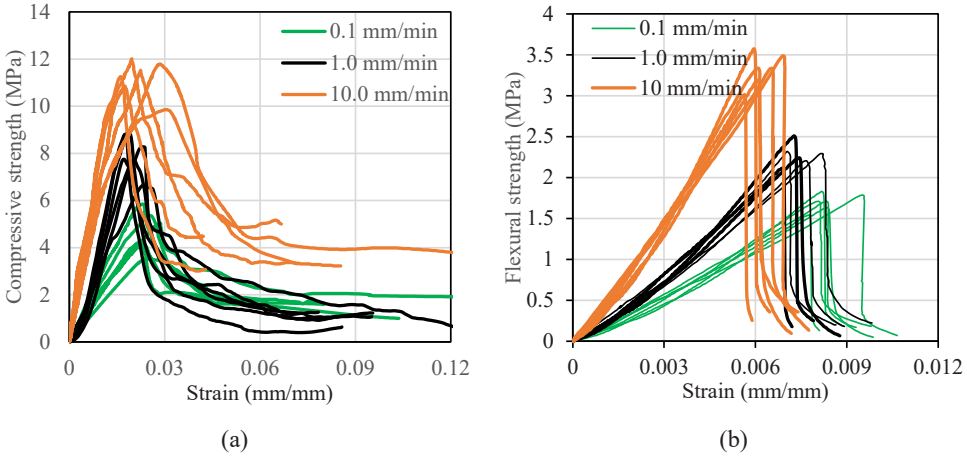

Fig. 4. Stress strain curves of mortar beams under (a) uniaxial compression and (b) flexure.

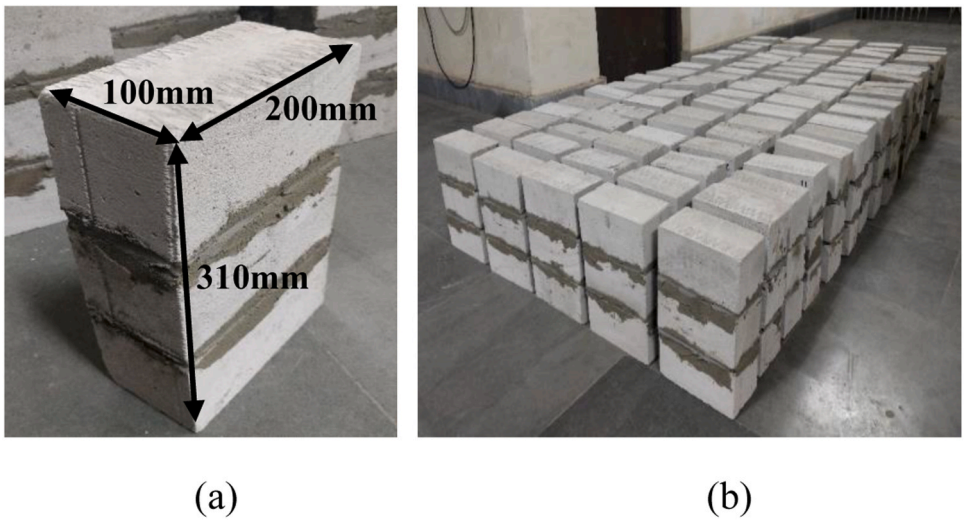

Fig. 5. Masonry triplet specimens (a) dimension details (b) AAC triplets.

Table 3
Details of specimen group classification.

Specimen Group	Displacement rate (mm/min)	Pre-compression (MPa)
Gr-1	0.1	0
Gr-2	0.1	0.2
Gr-3	0.1	0.6
Gr-4	0.1	1.0
Gr-5	1.0	0
Gr-6	1.0	0.2
Gr-7	1.0	0.6
Gr-8	1.0	1.0
Gr-9	10.0	0
Gr-10	10.0	0.2
Gr-11	10.0	0.6
Gr-12	10.0	1.0

no specific recommendation for laboratory tests of AAC masonry assemblages. Therefore, the present study considered the recommendation of IS 1905 [51] for burnt clay brick masonry, and, accordingly, stack-bonded prism specimens of size 310 × 200 × 100 mm^3 were considered for evaluation of the shear bond strength of AAC block masonry. Brick specimens of size 200 × 100 × 100 mm^3 were cut from AAC blocks using the diamond blade cutter and hacksaw and used to fabricate stack-bonded brick masonry triplet specimens (108 numbers) of dimensions 310 × 200 × 100 mm^3 as shown in Fig. 5. The brick units are bonded with premixed mortar-specific types of block adhesive (Titan Bond), and the thickness of the mortar-brick joints is kept between 2 to 5 mm. The block adhesive used in this study was a commercially available jointing material conforming to ANSI A118.4 [52]. It was a factory-prepared mixture of Portland cement, graded aggregates, and polymers designed for use with water to produce a high-strength thixotropic mortar. After fabrication, all the masonry specimens were cured under ambient conditions in the laboratory for 28 days before testing. After curing, masonry specimens are used for the experimental investigation to understand the effect of pre-compression and displacement rates on the monotonic shear mechanical test. All specimens were divided into 12 groups based on the combination of the effect of displacement rates ranging from 0.1 to 10 mm/min and pre-compressions from 0 to 1 MPa as shown in Table 3. Nine specimens were prepared for each of these 12 groups (Gr. 1–12), accounting a total of 108 specimens.

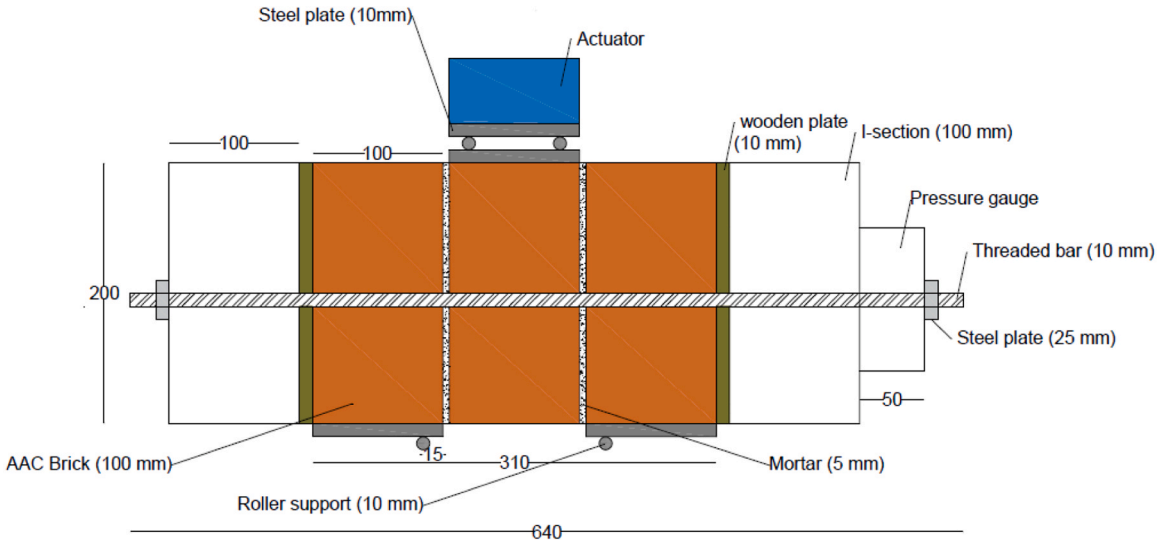

Fig. 6. Schematic diagram of test setup for the shear strength of masonry triplet specimens.

3.4. Instrumentation and test setup

It is required to apply loads in two axes (pre-compression on the horizontal axis and shear load on the vertical axis) on the specimen independently and simultaneously. There were two different test setups for handling this complex issue, viz., by using servo-controlled actuators for applying pre-compression and the shear load, or by using reaction-based rigs that can hold specimens tightly and apply the required level of pre-compression through screw mechanism, after which the shear load is applied using compression testing machine. To determine the shear bond strength, a displacement controlled UTM (with a maximum load capacity of 100 kN) was used to test all specimens. As discussed in the introduction section, there is a need for a suitable test set-up for applying constant pre-compression while applying shear force. For this purpose, a novel 'masonry triplet shear frame' (see Fig. 6) was designed and fabricated specifically for carrying out the shear test on masonry triplets. The assembly of the shear frame configuration consists of the following nine primary components: (1) rectangular steel base plate (2) four roller supports (12 mm dia.), (3) four thin plates (100 ×100 ×12 mm^3), (4) two bar (16 mm dia., 1000 mm long), (5) two I-sections (ISMB 200), (6) two wooden plates (200 ×100 ×25 mm^3), (7) two steel plate (200 ×100 ×25 mm^3), (8) dial gauge and (9) hydraulic jack. These components are marked with the serial number written above in Fig. 7. The components are fabricated and assembled in the

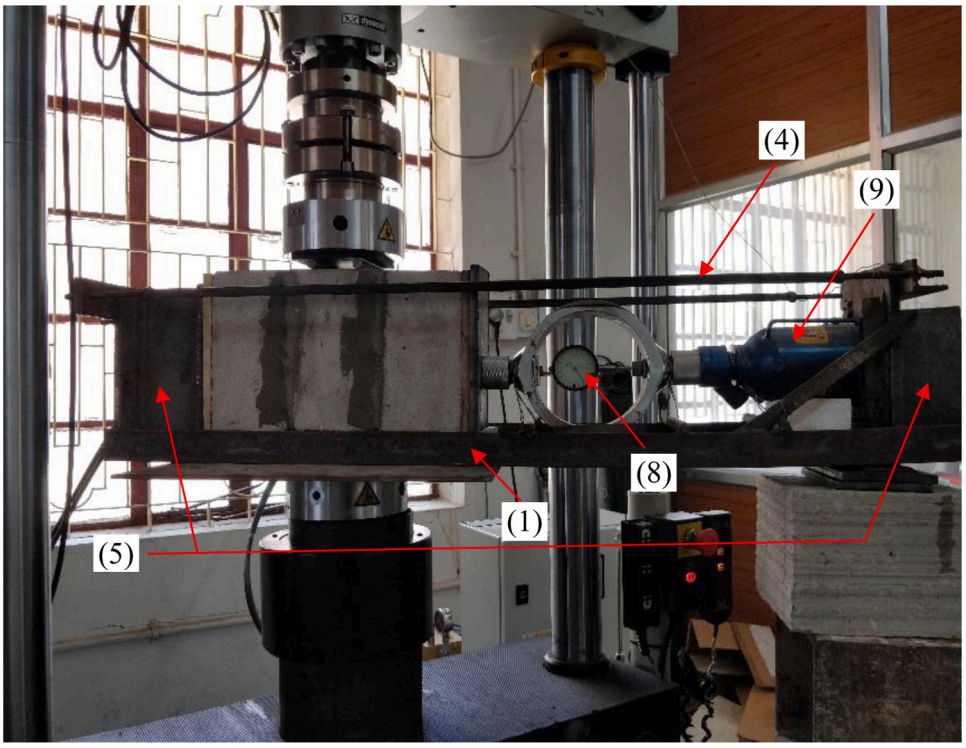

(a)

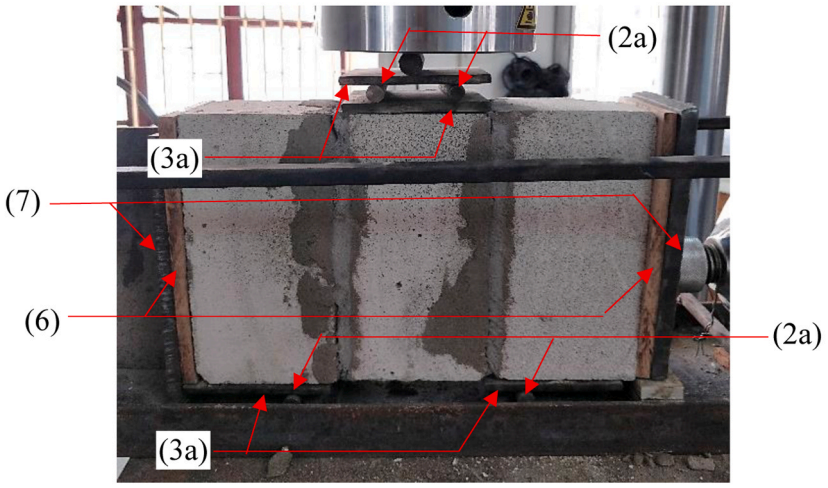

(b)

Fig. 7. (a) Masonry triplets positioned in the testing machine; and (b) different components of the test setup.

laboratory. Two I-Section (5) were fixed at each end of the rectangular base plate (1) and the bars (4) were connected side by side at the top of the I-section. The hydraulic jack (9) and dial gauge (8) were attached to the right side of the rectangular base plate to provide the pre-compression. This shear frame applies the pre-compression manually through a hydraulic jack mechanism. Next, the AAC masonry triplet is placed on the thin plates (4) with roller supports (2) so that the specimens are subjected to a 4-point bending load. Two wooden plates (6) and two steel plates (7) were placed on both sides of the AAC masonry triplet to minimize friction or slippage. The shear frame is therefore ready with the test specimen (held in a selected pre-compression) and can now be placed in the UTM for shear testing. The vertical load is applied by the UTM in the middle of the central brick of the triple specimen, while the two outer bricks are held on the roller supports (2).

4. Test results

Three displacement rates (i.e., 0.1, 1.0, and 10 mm/min) are considered in this study. As discussed above, the shear test was conducted at four different constant pre-compressions (i.e., 0, 0.2, 0.6, and 1.0 MPa). The shear bond strength is evaluated [14,34] as follows.

$$\tau = \frac{P_{\max}}{2A_c} \tag{4}$$

Where τ is the shear bond strength, $P_{\max}$ is the peak vertical load applied by the UTM and A_c is the contact area. The test results for the AAC masonry assemblages are presented in the following subsections.

The deformations of the central (middle) brick relative to the outer bricks were measured using UTM. The movement of the hydraulic piston corresponds to the displacement of the middle brick, and the shear strain

Table 4
Experimental outcomes from the shear test of AAC triplets.

Displacement rate (mm/min)	σ_{hp} (MPa)	$P_{\max}$ (N)	ε (mm/mm)	τ (MPa)
0.1	0.0	1684 (0.07)	0.0330 (0.11)	0.042 (0.07)
	0.2	14138 (0.10)	0.0343 (0.39)	0.353 (0.10)
	0.6	20270 (0.10)	0.0364 (0.19)	0.507 (0.10)
	1.0	27808 (0.07)	0.0422 (0.19)	0.695 (0.07)
1	0.0	2890 (0.08)	0.0403 (0.09)	0.072 (0.08)
	0.2	19552 (0.12)	0.0269 (0.14)	0.489 (0.12)
	0.6	28164 (0.06)	0.0376 (0.18)	0.704 (0.06)
	1.0	37517 (0.08)	0.0364 (0.31)	0.938 (0.08)
10	0.0	4295 (0.13)	0.0298 (0.13)	0.107 (0.09)
	0.2	22537 (0.19)	0.0175 (0.45)	0.563 (0.19)
	0.6	32368 (0.11)	0.0263 (0.30)	0.809 (0.11)
	1.0	42263 (0.08)	0.0288 (0.29)	1.056 (0.08)

Note: The values in the parenthesis represent the coefficient of variations

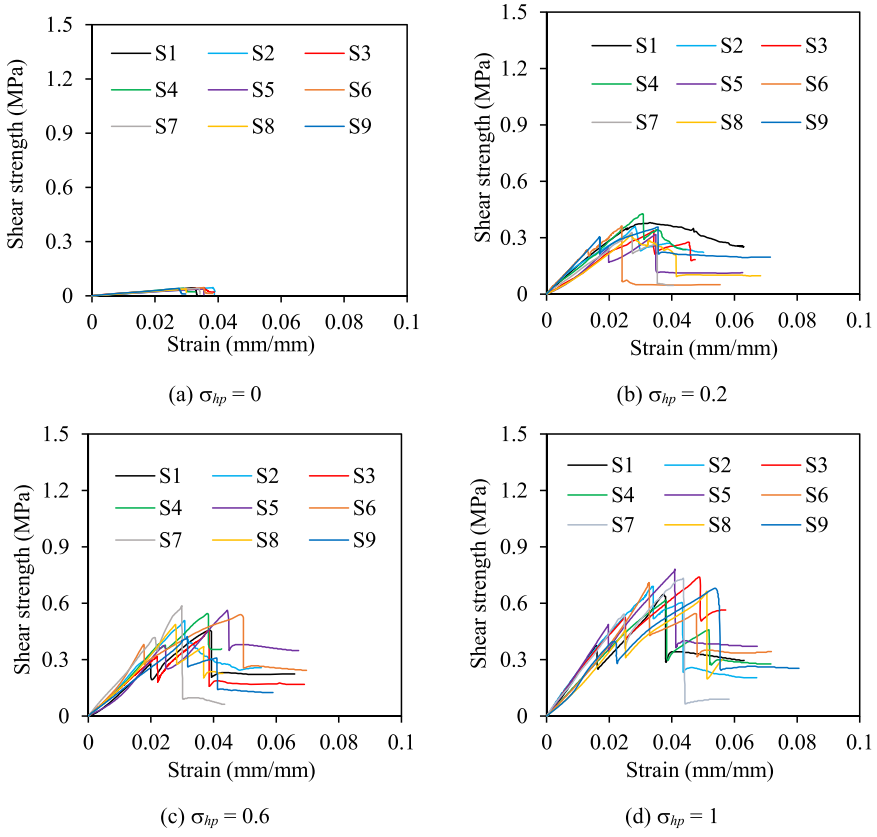

Fig. 8. Stress-strain characteristics of AAC masonry triplets at 0.1 mm/min displacement rate.

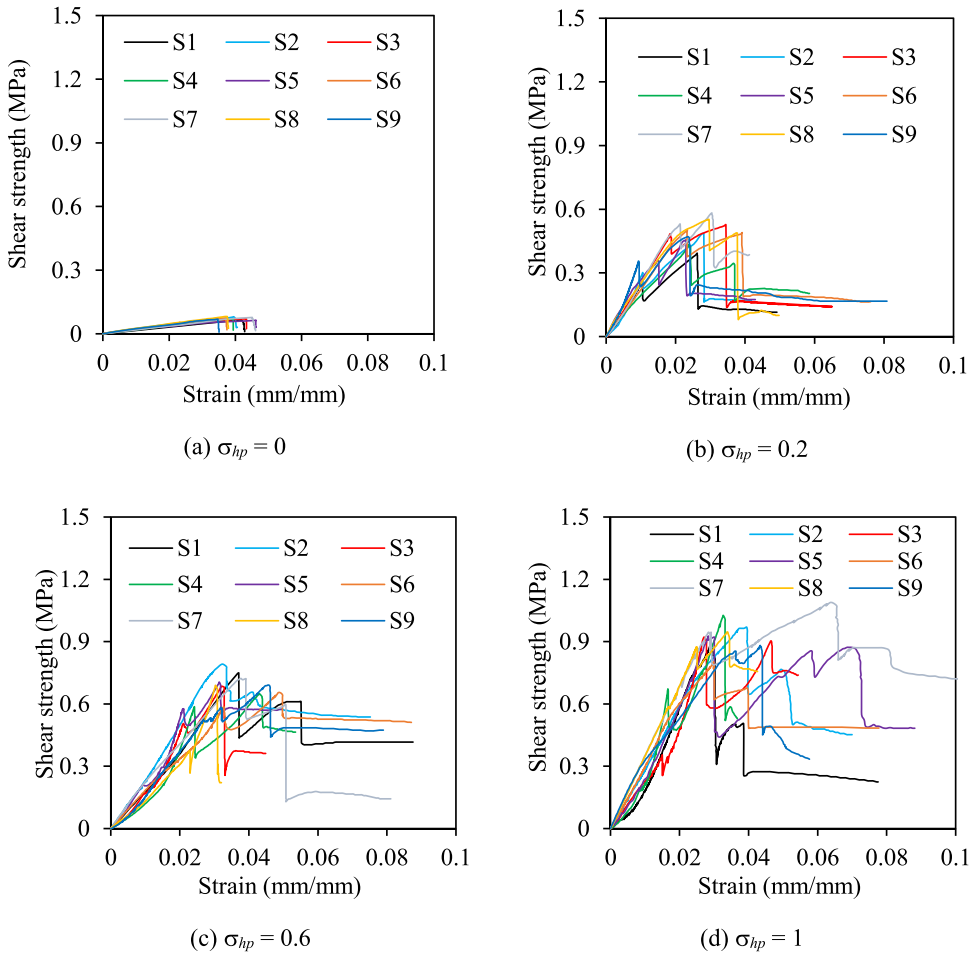

Fig. 9. Stress-strain characteristics of AAC masonry triplets at 1 mm/min displacement rate.

is computed based on the displacement of the middle brick relative to the outer brick in the triplet specimen. Table 4 shows the peak load (P_{max}), strain at peak load (ε), and shear bond strength (τ) exhibited during the monotonic shear test for different combinations of loading rates and pre-compressions (σ_{hp}) for AAC triplets (more information available in Table A in Appendix). From Table 4, it is observed that the peak load and shear bond strength increase with the increase in the loading rates. In addition, it is also reported that both peak load and shear bond strength increase as the pre-compression stress increases. Figs. 8–10 show the stress-strain curves of AAC masonry triplet specimens under bond shear stress with different displacement rates and pre-compressions.

Fig. 11 illustrates the relationship between the peak shear strengths (see Table 4), calculated as the ratio between the peak shear strength and two times the cross-sectional area of the interface, and the pre-compression stress under monotonic loading. The peak shear strength for the selected levels of pre-compressions (0, 0.2 MPa, 0.6 MPa, 1.0 MPa) can be interpolated with a straight line, representing the Mohr-Coulomb failure criterion. This is expressed as:

$$\tau = c + \sigma_{hp}\tan(\phi) \tag{5}$$

where σ_{hp} is the pre-compression, c is the cohesion, and ϕ is the friction angle. Table 5 shows the values of cohesion and friction angle providing the best fit of Eq. 5 to the experimental data. The values of the cohesion and friction obtained for the mortar joints are comparable to those obtained experimentally by Bhosale et al., [34] and Raj et al. [35,36]. It is interesting to note that the cohesion and friction angle values calculated with and without considering zero pre-compression lead to a significantly different result. The R^2 value indicates that the linear regression predictions fit the data perfectly well when zero pre-compression is not considered. In that case, it is found that the estimated cohesion value is considerably higher, and the friction angle is considerably lesser than that with zero pre-compression.

5. Failure pattern

Masonry triplets show different failure modes during the shear test and can be broadly categorized into the following three types: (a) slipping at the interface between the bricks and the mortar joints (b) failure of AAC block and (c) failure of mortar. Figs. 12–14 show the comparison of failure modes observed in AAC masonry triplets with different combinations of loading rates and pre-compressions. Most of the failure modes at lower loading rates can be characterized by slipping at the interface between the bricks and the mortar joints. This agrees also with EN 1052–3 [52] which states that slipping at the brick-mortar interface, and diagonal failure of the mortar joints (see Fig. 15) is the most common failure of AAC masonry. As the loading rate increases, other types of failure modes (such as AAC block failure and mortar failure) also begin to appear in equal numbers. Sometimes a combination of the two failure modes (as categorized above) is also observed. It was found that the higher the displacement rate, the more severe the failure. Higher pre-compression was found to impart a failure mode in masonry triplets involving the crushing of AAC blocks.

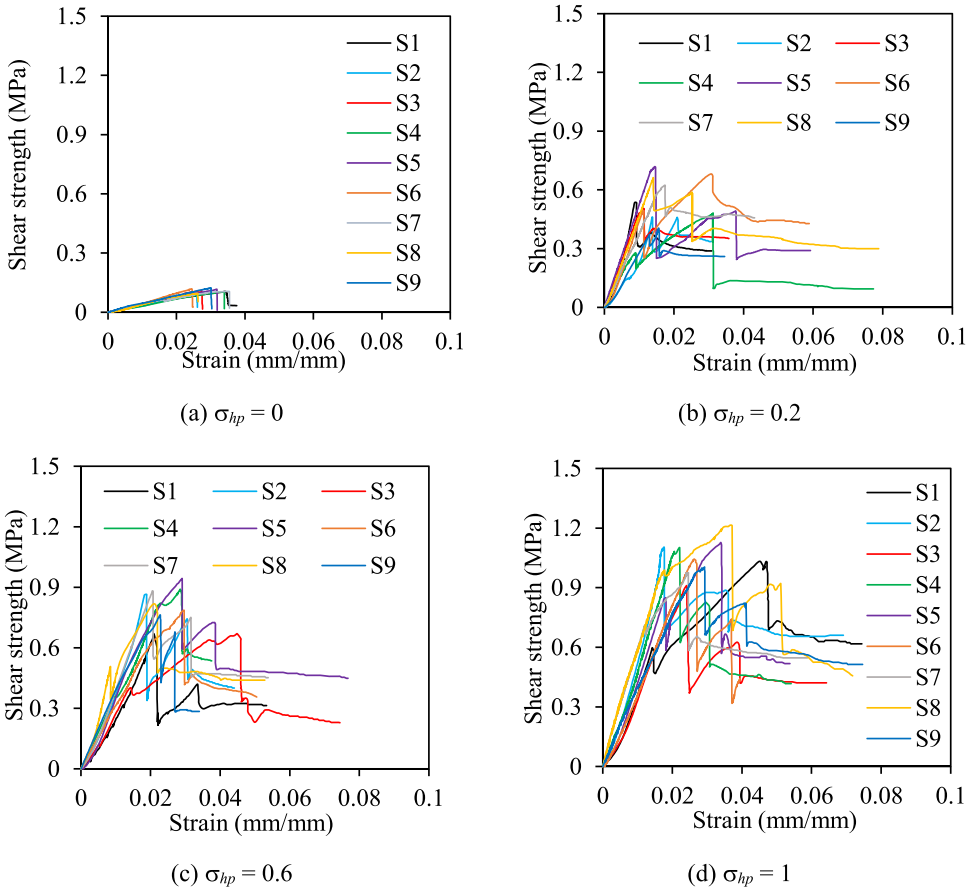

Fig. 10. Stress-strain characteristics of AAC masonry triplets at 10 mm/min displacement rate.

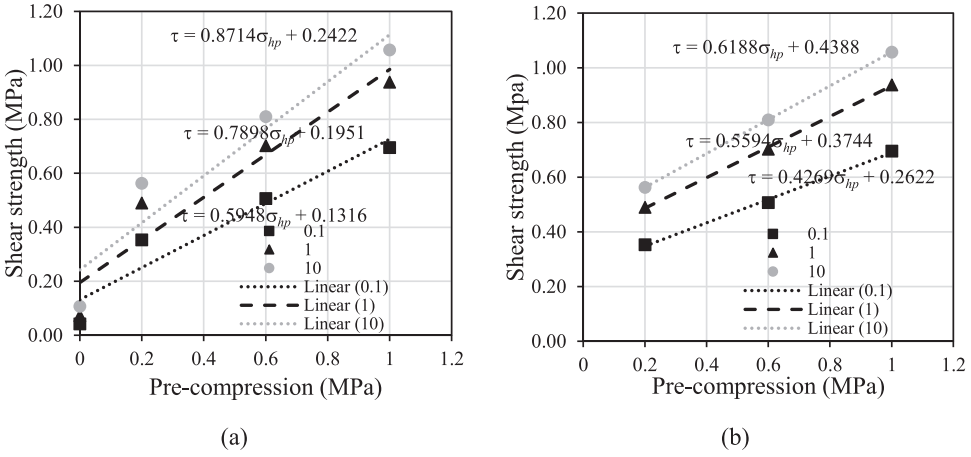

Fig. 11. Relationship between AAC shear strength and pre-compression stress under monotonic loading; (a) with and (b) without considering zero pre-compression.

Table 5
Shear strength model of AAC triplets with and without considering zero pre-compression.

Displacement rate (mm/min)	Considering zero pre-compression		Without zero pre-compression	
	ϕ (deg.)	c (MPa)	ϕ (deg.)	c (MPa)
0.1	30.74	0.13	23.12	0.26
1	38.30	0.19	29.22	0.37
10	41.07	0.24	31.75	0.44

(a) σ_{hp} = 0 MPa (b) σ_{hp} = 0.2 MPa

(c) σ_{hp} = 0.6 MPa (d) σ_{hp} = 1 MPa

Fig. 12. Failure pattern of AAC masonry triplets at load rate 0.1 mm/min.

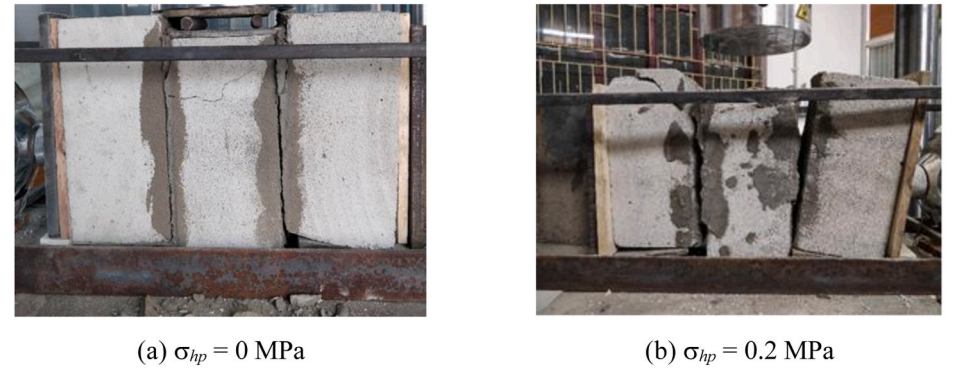

(a) σ_{hp} = 0 MPa (b) σ_{hp} = 0.2 MPa

(c) σ_{hp} = 0.6 MPa (d) σ_{hp} = 1 MPa

Fig. 13. Failure pattern of AAC masonry triplets at load rate 1 mm/min.

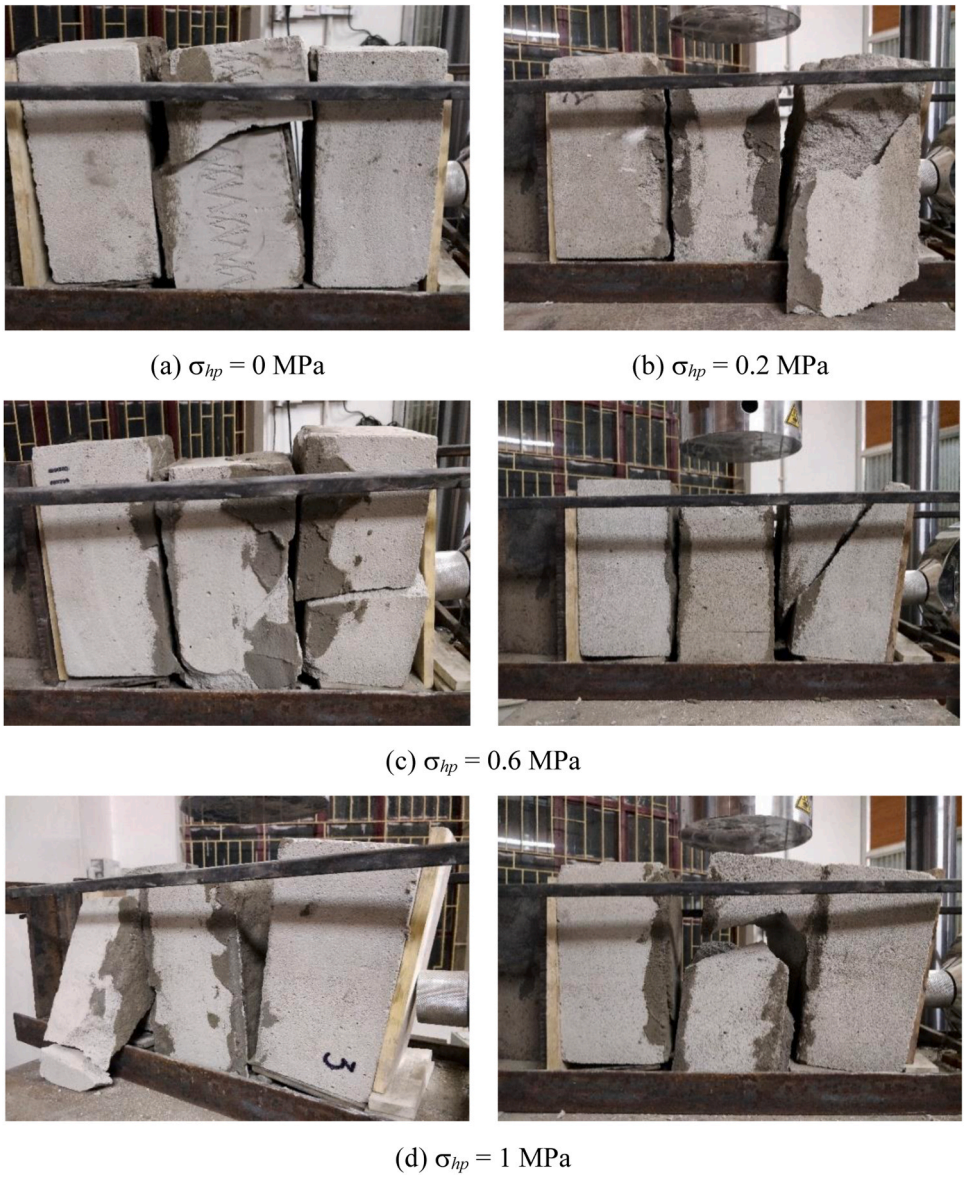

Fig. 14. Failure pattern of AAC masonry triplets at load rate 10 mm/min.

6. Numerical calibration

The shear test results of AAC masonry triplets are considered for the numerical calibration study using Abaqus [53], which is a commercially available finite element (FE) software. The idea is to identify and predict the locations of the critical internal stresses and strains developed within the masonry which is not possible to identify during the experimental tests. It can also help in numerically simulating the experimentally obtained progressive crack/failure developed in the AAC masonry. This proposed numerical analysis uses a micro modelling strategy which treats masonry units and mortar as an anisotropic continuum that are discretized using 20-noded (C3D20R: A 20-node quadratic element with reduced integration) three-dimensional solid elements.

The proposed FE model considers a displacement-controlled loading scheme where the behaviour of the material follows the Concrete Damage Plasticity (CDP) model [54]. The CDP model uses the modified Kent-Park model [55] to develop the equivalent backbone curve under compression for both AAC masonry units and mortar joints.

Surface-to-surface contact cohesive interfaces are used to simulate the bond between the AAC unit and mortar layers. The cohesive interfaces initially exhibit a linear elastic response, followed by a cracking behaviour that describes the most critical failure modes, namely, tensile cracking and shear sliding. This allows simulating the failure occurred in correspondence of the brick-mortar interfaces for the masonry prisms. The cohesive behaviour is controlled by the stiffness along the direction normal to the joint, k_n, and along two orthogonal shear directions in the plane of the joint, k_s and k_t. The values of the joint stiffnesses depend on the elastic properties of the components and on the geometry of the joints [42]. Table 6 illustrates the main parameters describing the interaction properties.

Fig. 16 shows the FE model of the AAC triplet developed consisting of AAC unit and ready-mix mortar. Finer mesh element discretization of size 10 mm is selected for the accurate prediction of shear strength. The stress-strain responses of the developed FE models with varying load rates as well as varying pre-compression levels are compared with the experimental outcomes and a fair match is established as seen in Figs. 17–20.

To study the gradual development of stress and strain within masonry components as well as mortar unit joints, and to identify failure locations, peak compressive and plastic strain contours are developed for a strain limit of 0.02 (corresponds to displacement of 4 mm). Fig. 21 shows the plastic strain distribution subjected to zero pre-compression

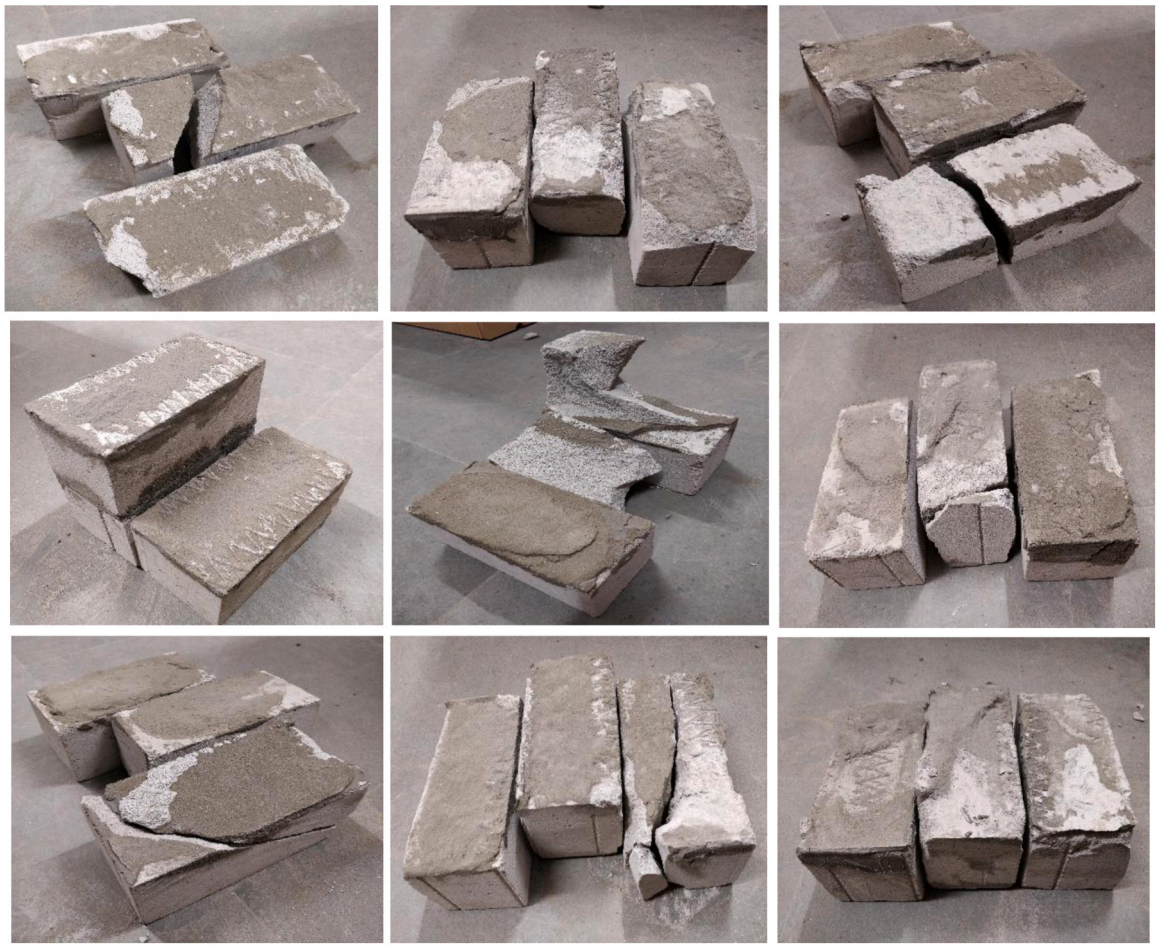

Fig. 15. Typical failure modes observed in the AAC specimens.

Table 6
Brick-mortar joint interaction properties.

Mortar Interaction Properties	Brick-mortar joints	Source
k_n per unit area (N/mm^3)	1000	[56,57]
k_s per unit area (N/mm^3)	500	[56,57]
k_t per unit area (N/mm^3)	500	[56,57]
Masonry Tensile strength, σ_t (MPa)	0.3	[34–36]
Cohesion, c (MPa)	0.4	[34–36]
Coefficient of friction, μ (-)	0.6	[34–36]
Normal fracture energy per unit area, G_f^I(MPa-mm)	0.015	[56,57]
Shear fracture energy per unit area, G_f^{II} (MPa-mm)	0.09	[56,57]

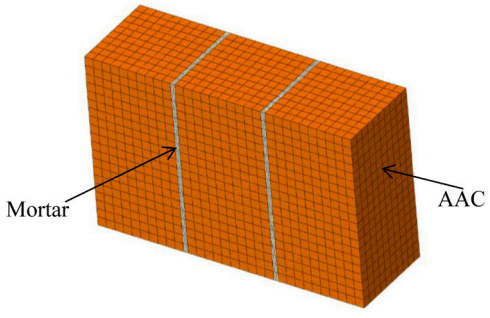

Fig. 16. Micro scale consideration of triplets.

for 0.1, 1.0 and 10 mm/min displacement rates. In the absence of pre-compression, the failure is found to be occurring in either of the two mortar-brick interfaces and once the failure occurs, it propagates until the complete failure is attained. Although higher magnitude of strains is obtained for the displacement rate of 10 mm/min (Fig. 21c), still, no significant difference in the deformed shape and distributions of maximum plastic strains are visible. However, while comparing the peak compressive stresses (Fig. 22), for all selected loading rates, a visible increase in the maximum stress zones can be seen with increasing loading rates. Again, the high-concentration stress contours are more irregular at the highest selected displacement rate (10 mm/min) due to the development of sudden dynamic and irregular loading as compared to the 0.1 and 1 mm/min displacement rates (refer to Figs. 22b, c).

Fig. 23 shows the plastic strain distribution for varying loading rates

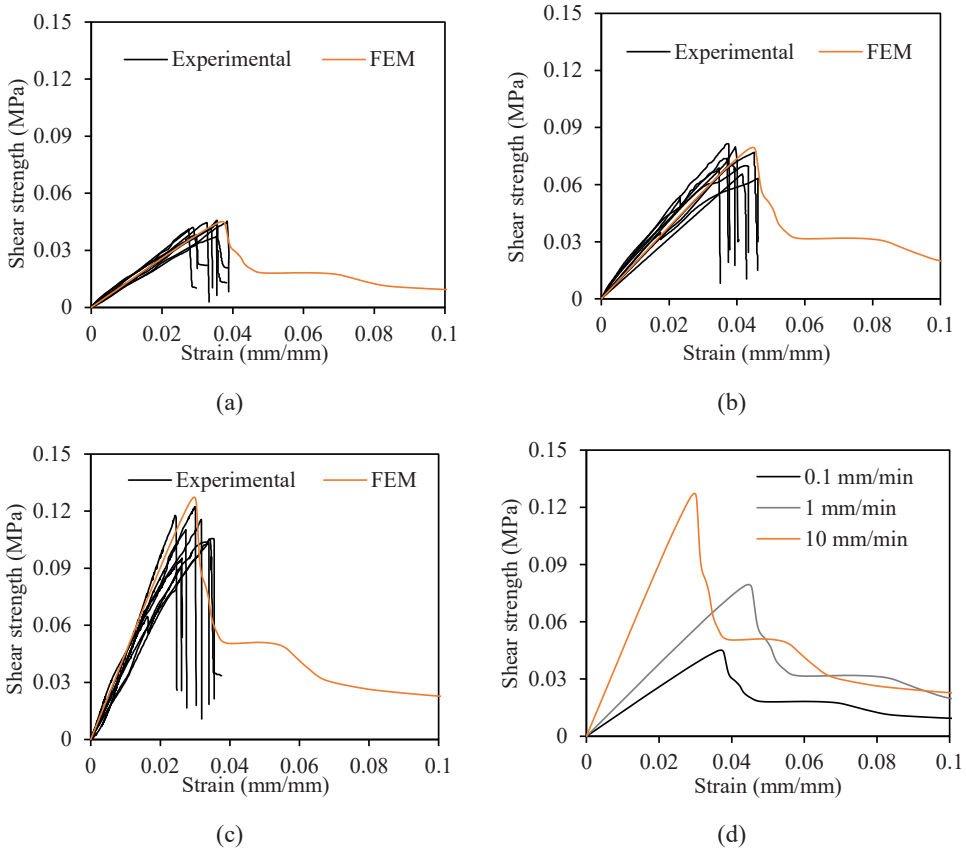

Fig. 17. Stress-strain characteristics of masonry triplets at load rates (a) 0.1 (b) 1.0 (c) 10.0 mm/min (d) all loading rates with $\sigma_{hp} = 0$ MPa.

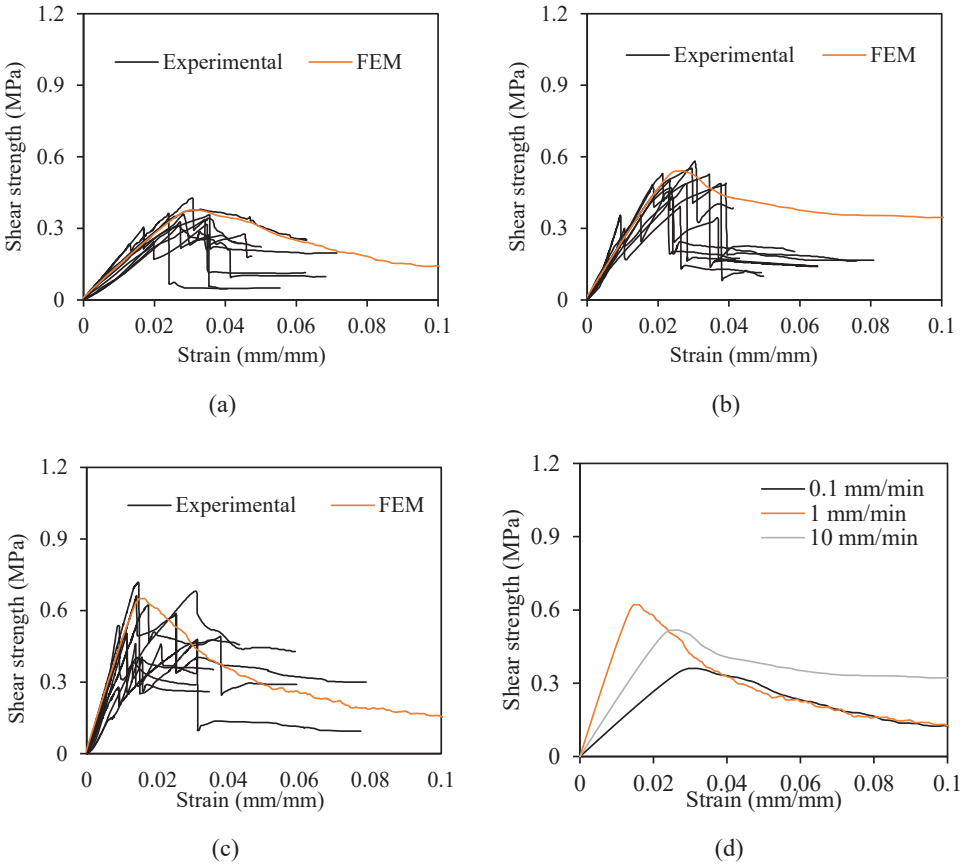

Fig. 18. Stress-strain characteristics of masonry triplets at load rates (a) 0.1 (b) 1.0 (c) 10.0 mm/min (d) all loading rates with $\sigma_{hp} = 0.2$ MPa.

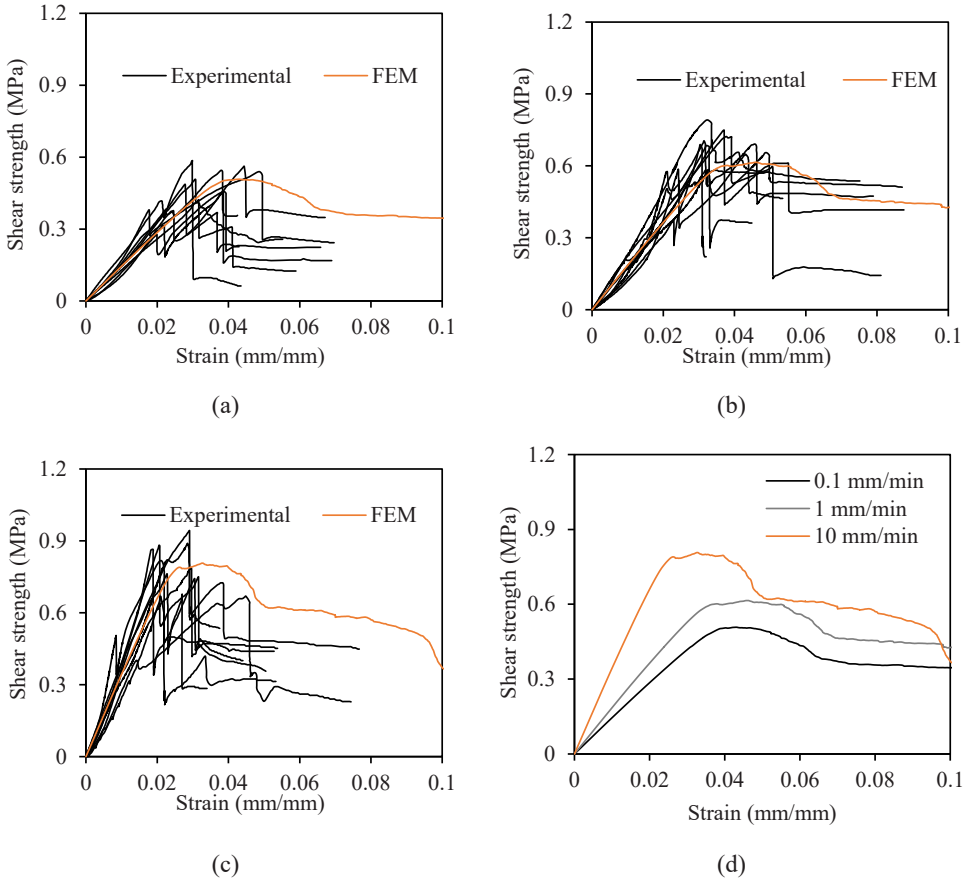

Fig. 19. Stress-strain characteristics of masonry triplets at load rates (a) 0.1 (b) 1.0 (c) 10.0 mm/min (d) all loading rates with $\sigma_{hp} = 0.6$ MPa.

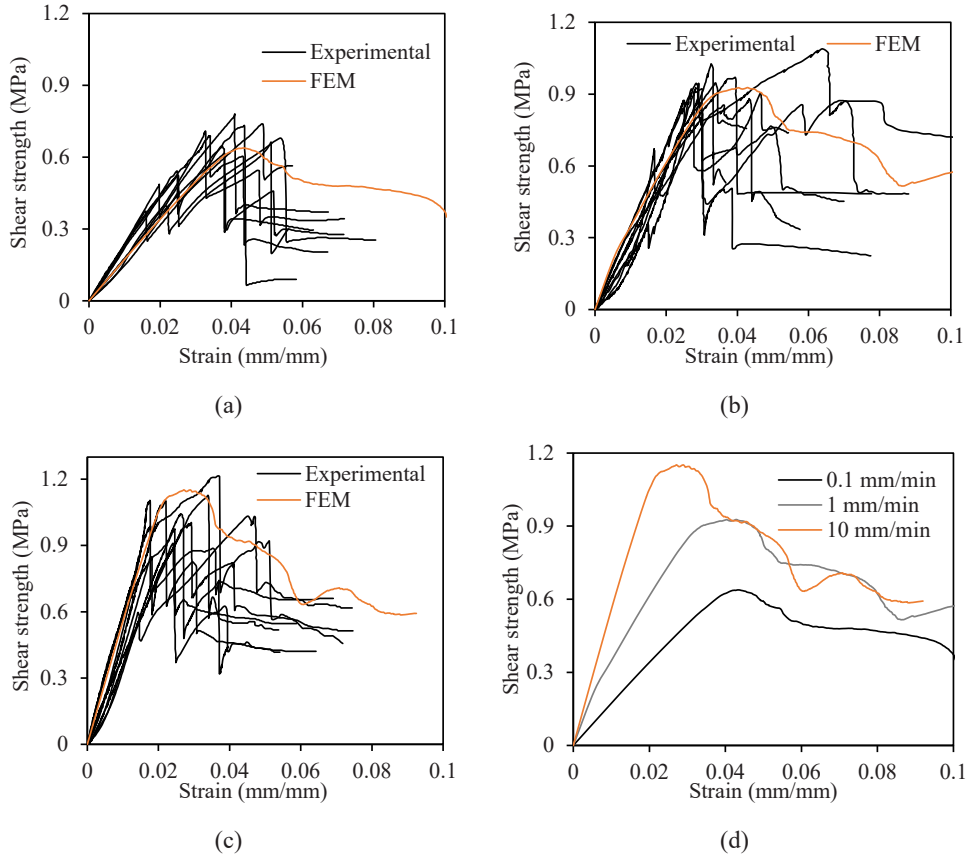

Fig. 20. Stress-strain characteristics of masonry triplets at load rates (a) 0.1 (b) 1.0 (c) 10.0 mm/min (d) all loading rates with $\sigma_{hp} = 1.0$ MPa.

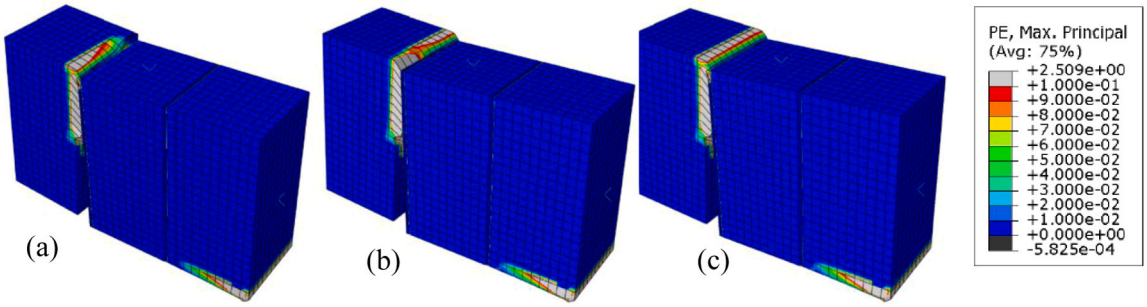

Fig. 21. Distribution of plastic strain at load rates (a) 0.1 (b) 1.0 (c) 10.0 mm/min with no pre-compression.

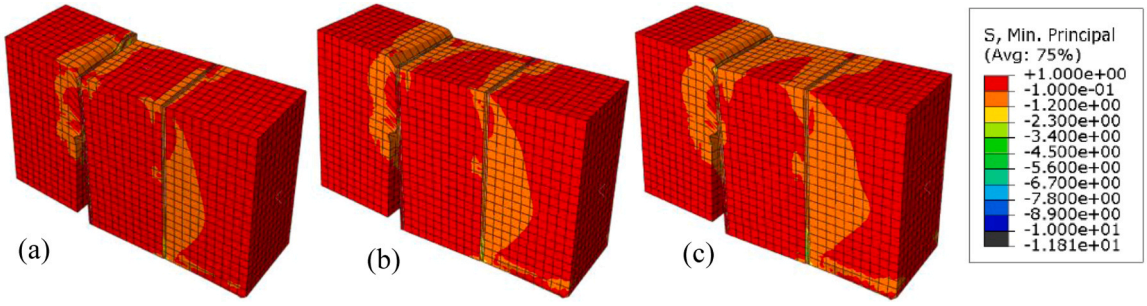

Fig. 22. Distribution of minimum principal stress at load rates (a) 0.1 (b) 1.0 (c) 10.0 mm/min with no pre-compression.

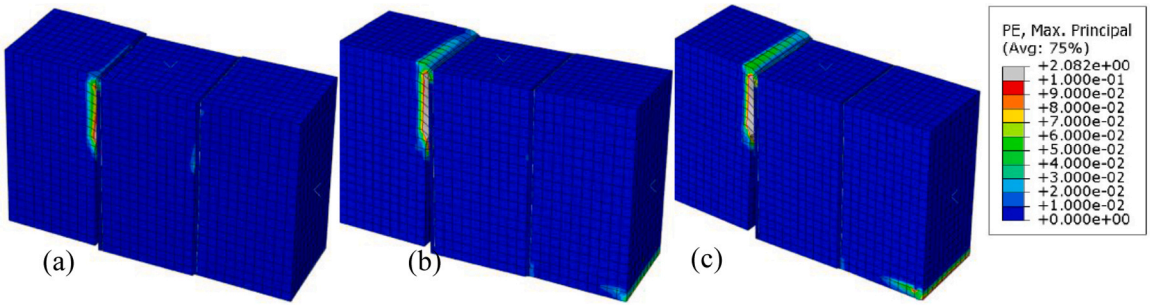

Fig. 23. Distribution of plastic strain at load rates (a) 0.1 (b) 1.0 (c) 10.0 mm/min with 0.2 pre-compression.

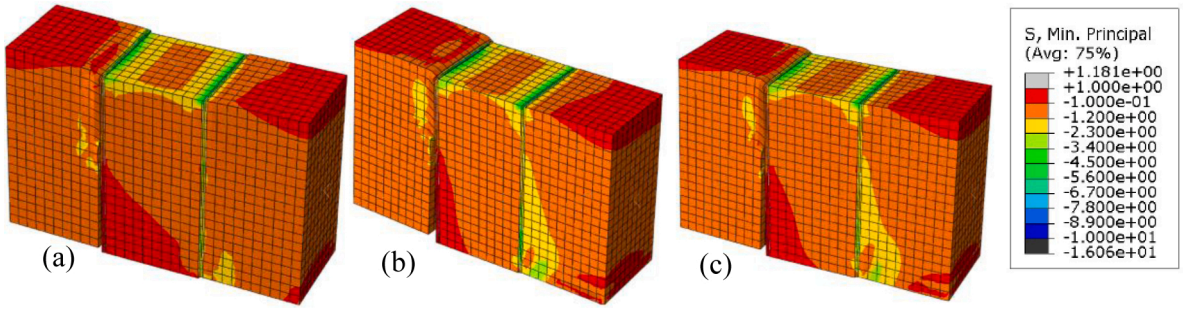

Fig. 24. Distribution of minimum principal stress at load rates (a) 0.1 (b) 1.0 (c) 10.0 mm/min with 0.2 MPa pre-compression.

at a horizontal pre-compression of 0.2 MPa. Compared to, Fig. 21, due to presence of a pre-compression, lower strain magnitudes are visible, and which are distributed in lesser areas. Again, the outer brick connected to the unaffected mortar-brick joint (Fig. 23) is found to be having lesser magnitude of strains as compared to those presented in Fig. 22. Fig. 24 shows the peak principal stress distributions at varying loading rates for 0.2 MPa of pre-compression. The highest stress concentrations are visible in Fig. 24c followed by Fig. 24b and a.

On further increase in pre-compression (i.e., 0.6 and 1.0 MPa), lesser damage in the interfaces and almost no corner crushing of the masonry units is visible as seen in Figs. 25 and 27 showing the plastic strain deformations. Compared to Figs. 21 and 23, no significant damage in the brick units is visible in Fig. 25a. Again, the failure is visible in both the mortar-brick interfaces although one of the interfaces is significantly more damaged than the other (See Fig. 25).

Fig. 27a shows lowest levels of plastic strain as compared to Figs. 27b, c. Fig. 26 and Fig. 28 show the peak compressive strength distribution at a pre-compression of 0.6 MPa and 1.0 MPa respectively. Unlike, Figs. 22 and 24, the maximum stress contours are distributed between two of the mortar-brick interfaces rather than being

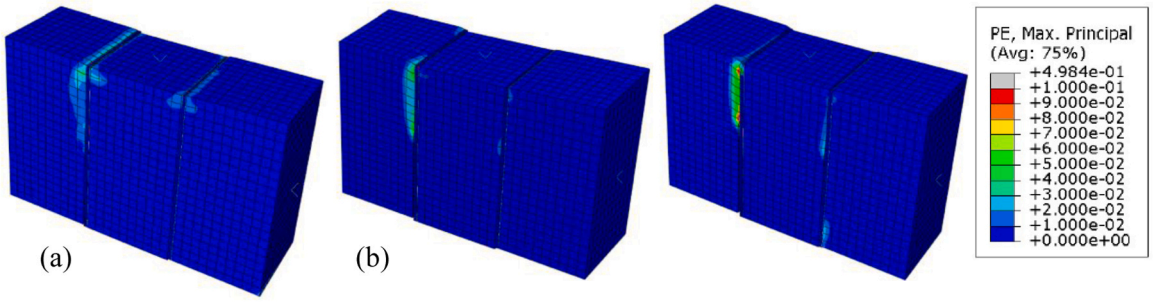

Fig. 25. Distribution of plastic strain at load rates (a) 0.1 (b) 1.0 (c) 10.0 mm/min with 0.6 MPa pre-compression.

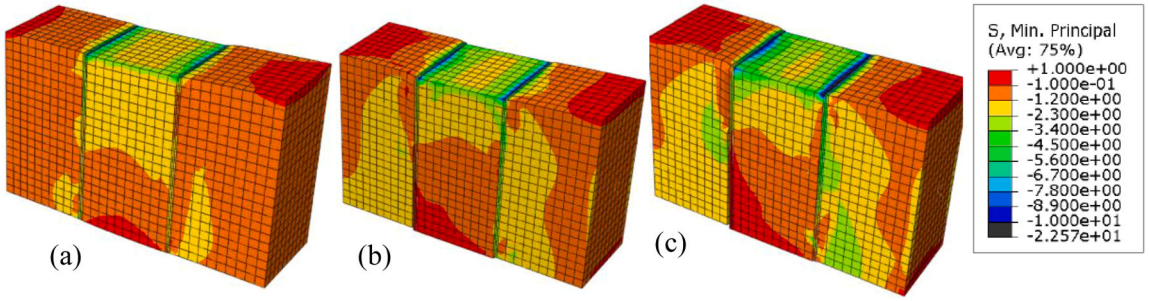

Fig. 26. Distribution of minimum principal stress at load rates (a) 0.1 (b) 1.0 (c) 10.0 mm/min with 0.6 MPa pre-compression.

0.6 MPa pre-compression.

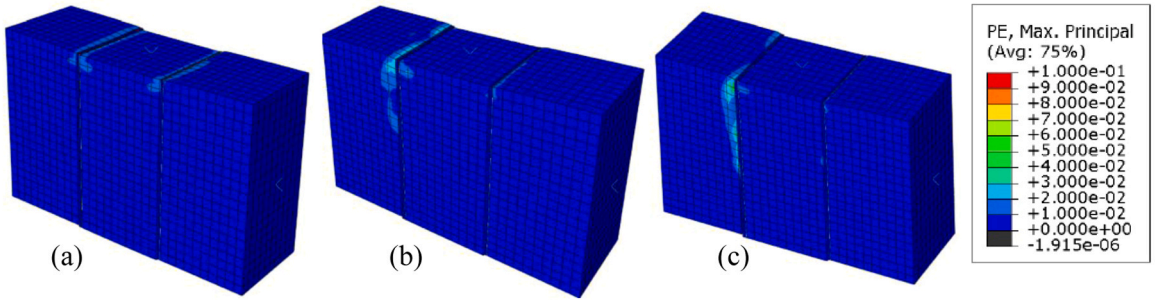

Fig. 27. Distribution of plastic strain at load rates (a) 0.1 (b) 1.0 (c) 10.0 mm/min with 1.0 MPa pre-compression.

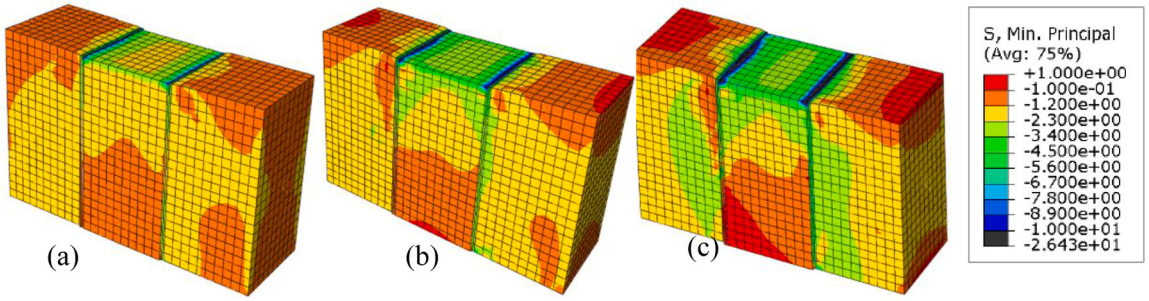

Fig. 28. Distribution of minimum principal stress at load rates (a) 0.1 (b) 1.0 (c) 10.0 mm/min with 1.0 MPa pre-compression.

concentrated in either of the interfaces. Again, with increase in the loading rate, higher peak stress concentrations are visible (see Figs. 26 and 28). Lastly, the deformed shape identified in Figs. 21–28 are found to be identical to the experimentally obtained failed specimens seen in Figs. 12–14.

7. Conclusion

This study investigates the shear strength of AAC masonry subjected to various levels of pre-compression considering low to high load rates followed by a numerical micro-scale modelling. The result of this study will help to evaluate the shear capacity more accurately and thus help to better evaluate the safety of AAC block masonry structures. Masonry

walls are likely to experience very high loading rates during storm winds and earthquakes. Therefore, it is of considerable importance to understand the shear behavior of AAC block masonry under different loading rates. To provide further insights into the behaviour, complementary non-linear numerical simulations are performed, using key parameters obtained from laboratory experiments. The numerical models employ detailed surface-based cohesive contact approaches, taking due account of inelastic damage at masonry interfaces and damage plasticity modeling for the constitutive response of brick materials. It is shown that the adopted numerical approaches can reliably capture the main behavioral characteristics and failure modes and can therefore be employed for further numerical evaluations.

In this study, AAC blocks sourced from the same batch were used to ensure consistency and reliability in the experimental approach mitigating potential variations in their properties attributable to the manufacturing process. The mortar used in preparing the masonry triplets adhered to the ANSI A118.4 [52], ensuring conformity to established quality norms. To align with relevant codes and published literature, all masonry specimens in this investigation featured mortar joints of 3–5 mm thickness. Three distinct loading rates were considered to comprehensively assess the shear-bond strength of AAC masonry assemblies. Additionally, the finite element modelling and analysis were performed using Abaqus software, offering a robust computational framework for the study. The key outcomes of the present study are highlighted as follows:

- Peak load and shear bond strength are observed to increase with increasing loading rates, leading to severe failure at higher loading rates.
- Higher pre-compression was found to impart a failure mode in masonry triplets involving the crushing of AAC blocks.
- In the absence of pre-compression, the failure is found to be occurring in either of the two mortar-brick interfaces and once the failure occurs, it propagates until the complete failure is attained irrespective of the applied loading rate. However, while comparing the peak compressive stresses for all selected loading rates, a visible increase in the maximum stress zones can be seen with increasing loading rates.
- High-concentration stress contours are more irregular at the highest selected displacement rate (10 mm/min) due to the development of sudden dynamic and irregular loading as compared to the 0.1 and 1 mm/min displacement rates.
- As the pre-compression increases, lower strain magnitudes are visible as compared to the case of zero pre-compression and are distributed in lesser areas.
- Higher pre-compressions lead to lesser damage in the brick-mortar joint interfaces and corner crushing of masonry units. Failure is visible in both the mortar-brick interfaces although one of the interfaces is significantly more damaged than the other. The maximum stress contours are distributed between two of the mortar-brick interfaces rather than being concentrated in either of the interfaces.

The outcomes of this study will draw the attention of researchers and structural engineers while selecting mechanical strength parameters at both static and dynamic loading conditions and studying the performance-based design of framed buildings infilled with AAC block masonry. The potential of AAC masonry structures can be further investigated through a full-scale laboratory testing and comprehensive structural analysis. Several other properties like as thermal conductivity, sound insulation, chloride resistance, carbonation resistance, fire resistance, creep, and shrinkage, etc., can be investigated to better evaluate the effectiveness of AAC masonry.

CRediT authorship contribution statement

Devi Ningombam Reena: Writing – original draft, Visualization, Methodology, Formal analysis, Data curation, Conceptualization. **Dhir Prateek Kumar:** Writing – review & editing, Software. **Sarkar Pradip:** Writing – review & editing, Visualization, Supervision, Methodology, Investigation, Conceptualization.

Declaration of Competing Interest

The authors whose names are listed immediately below certify that they have NO affiliations with or involvement in any organization or entity with any financial interest (such as honoraria; educational grants; participation in speakers' bureaus; membership, employment, consultancies, stock ownership, or other equity interest; and expert testimony or patent-licensing arrangements), or non-financial interest (such as personal or professional relationships, affiliations, knowledge or beliefs) in the subject matter or materials discussed in this manuscript.

Data availability

Data will be made available on request.

Appendix

Table A
Experimentally obtained bond shear strength parameters of AAC triplets.

Group	Samples	Peak load (N)	Strain at peak load (mm/mm)	Bond shear strength (MPa)
Gr-1	S1	1786	0.0326	0.044
	S2	1815	0.0384	0.045
	S3	1740	0.0354	0.043
	S4	1684	0.0286	0.042
	S5	1484	0.0354	0.037
	S6	1833	0.0355	0.046
	S7	1637	0.0336	0.041
	S8	1527	0.0298	0.038
	S9	1651	0.0276	0.041
	Mean	1684	0.0330	0.042
	CV	0.07	0.11	0.72
Gr-2	S1	15204	0.0331	0.380
	S2	14373	0.0283	0.359
	S3	13502	0.0686	0.338
	S4	17092	0.0307	0.427
	S5	12642	0.0349	0.316

(*continued on next page*)

Table A (*continued*)

Group	Samples	Peak load (N)	Strain at peak load (mm/mm)	Bond shear strength (MPa)
	S6	14518	0.0240	0.363
	S7	13107	0.0272	0.328
	S8	12536	0.0267	0.313
	S9	14269	0.0356	0.357
	Mean	14138	0.0343	0.353
	CV	0.10	0.39	0.10
Gr-3	S1	18286	0.0387	0.457
	S2	20312	0.0307	0.507
	S3	18231	0.0383	0.456
	S4	21806	0.0380	0.545
	S5	22453	0.0444	0.561
	S6	21564	0.0484	0.539
	S7	23434	0.0299	0.586
	S8	19476	0.0279	0.487
	S9	16872	0.0316	0.422
	Mean	20270	0.0364	0.507
	CV	0.10	0.19	0.10
Gr-4	S1	25861	0.0372	0.647
	S2	27583	0.0341	0.690
	S3	29554	0.0485	0.739
	S4	24645	0.0379	0.616
	S5	31232	0.0410	0.781
	S6	28378	0.0327	0.710
	S7	29311	0.0437	0.733
	S8	26520	0.0512	0.663
	S9	27188	0.0538	0.679
	Mean	27808	0.04223	0.695
	CV	0.07	0.17	0.07
Gr-5	S1	2622	0.0416	0.066
	S2	3190	0.0396	0.080
	S3	2798	0.0426	0.069
	S4	2826	0.0380	0.071
	S5	2529	0.0463	0.063
	S6	2954	0.0372	0.074
	S7	3079	0.0451	0.077
	S8	3259	0.0373	0.081
	S9	2750	0.0348	0.068
	Mean	2890	0.0403	0.072
	CV	0.08	0.09	0.08
Gr-6	S1	15704	0.0262	0.393
	S2	19402	0.0279	0.485
	S3	21058	0.0345	0.526
	S4	17290	0.0237	0.432
	S5	18185	0.0230	0.455
	S6	20132	0.0234	0.503
	S7	23287	0.0304	0.582
	S8	22081	0.0296	0.552
	S9	18826	0.0236	0.471
	Mean	19552	0.0269	0.489
	CV	0.12	0.14	0.12
Gr- 7	S1	29946	0.0371	0.749
	S2	31673	0.0323	0.792
	S3	27407	0.0321	0.685
	S4	25944	0.0431	0.649
	S5	28195	0.0314	0.705
	S6	26204	0.0490	0.656
	S7	28901	0.0377	0.723
	S8	27568	0.0304	0.689
	S9	27638	0.0456	0.691
	Mean	28164	0.0376	0.704
	CV	0.06	0.18	0.06
Gr-8	S1	35213	0.0290	0.880
	S2	38777	0.0395	0.969
	S3	36844	0.0271	0.921
	S4	41036	0.0327	1.026
	S5	37068	0.0283	0.927
	S6	32125	0.0299	0.803
	S7	43526	0.0636	1.089
	S8	37822	0.0340	0.9456
	S9	35245	0.0434	0.881
	Mean	37517	0.0364	0.938
	CV	0.08	0.31	0.08
Gr-9	S1	4218	0.0342	0.105
	S2	3633	0.0259	0.091
	S3	4411	0.0273	0.110

(*continued on next page*)

Table A (*continued*)

Group	Samples	Peak load (N)	Strain at peak load (mm/mm)	Bond shear strength (MPa)
	S4	4134	0.0339	0.103
	S5	4620	0.0318	0.116
	S6	4712	0.0243	0.118
	S7	4223	0.0347	0.105
	S8	3813	0.0262	0.095
	S9	4891	0.0299	0.122
	Mean	4295	0.0298	0.107
	CV	0.13	0.13	0.09
Gr-10	S1	21440	0.0088	0.536
	S2	18454	0.0137	0.461
	S3	20216	0.0113	0.505
	S4	19183	0.0312	0.480
	S5	28704	0.0144	0.718
	S6	27235	0.0306	0.681
	S7	24947	0.0174	0.624
	S8	26494	0.0141	0.662
	S9	16156	0.0156	0.404
	Mean	22537	0.0175	0.563
	CV	0.19	0.45	0.19
Gr-11	S1	26720	0.0210	0.668
	S2	34587	0.0189	0.865
	S3	26770	0.0449	0.669
	S4	35601	0.0285	0.890
	S5	37704	0.0291	0.942
	S6	31447	0.0296	0.786
	S7	35259	0.0205	0.881
	S8	32715	0.0210	0.818
	S9	30511	0.0228	0.763
	Mean	32368	0.0263	0.809
	CV	0.11	0.30	0.11
Gr-12	S1	41284	0.045	1.03
	S2	44157	0.0176	1.10
	S3	36398	0.0241	0.91
	S4	43991	0.0221	1.09
	S5	45074	0.0339	1.13
	S6	41727	0.0262	1.04
	S7	38998	0.0241	0.98
	S8	48589	0.0369	1.21
	S9	40147	0.0292	1.00
	Mean	42263	0.0288	1.06
	CV	0.29	0.08	0.08

Note: CV represents the coefficient of variation

References

[1] A. Rahman, T. Ueda, Experimental investigation and numerical modeling of peak shear stress of brick masonry mortar joint under compression, J. Mater. Civ. Eng. 26 (9) (2014) 04014061.

[2] A. Ural, Triplet tests and numerical validations of stone masonry with dowels under shear, Arab. J. Sci. Eng. 46 (5) (2021) 4765–4779.

[3] G.P. van Zijl, Modeling masonry shear-compression: role of dilatancy highlighted, J. Eng. Mech. 130 (11) (2004) 1289–1296.

[4] P.B. Lourenço, J.O. Barros, J.T. Oliveira, Shear testing of stack bonded masonry, Constr. Build. Mater. 18 (2) (2004) 125–132.

[5] W.J. Cen, H. Wang, Y.J. Sun, L.S. Wen, Monotonic and cyclic shear behaviour of geomembrane-sand interface, Geosynth. Int. 25 (4) (2018) 369–377.

[6] A. Gabor, E. Ferrier, E. Jacquelin, P. Hamelin, Analysis and modelling of the in-plane shear behaviour of hollow brick masonry panels, Constr. Build. Mater. 20 (5) (2006) 308–321.

[7] Venkatarama Reddy, B. V., Lal, R., & Nanjunda Rao, K. S, Enhancing bond strength and characteristics of soil-cement block masonry, J. Mater. Civ. Eng. 19 (2) (2007) 164–172.

[8] B.V. Venkatarama Reddy, U. Vyas, Influence of shear bond strength on compressive strength and stress–strain characteristics of masonry, Mater. Struct. 41 (10) (2008) 1697–1712.

[9] Vermeltfoort, A.T. (2012). Shear strength variation due to mortar strength variation and the use of a triplet shear test set-up. In 15th International Brick and Block Masonry Conference. Florianopolis.

[10] S.B. Singh, P. Munjal, Bond strength and compressive stress-strain characteristics of brick masonry, J. Build. Eng. 9 (2017) 10–16.

[11] S.R. Balasubramanian, K.B. Rao, A.M. Prasad, R. Goswami, A comprehensive test procedure for determination of shear strength parameters of brick masonry specimens, J. Struct. Eng. 46 (5) (2019) 395–405.

[12] G. Sarangapani, B.V. Venkatarama Reddy, K.S. Jagadish, Brick-mortar bond and masonry compressive strength, J. Mater. Civ. Eng. 17 (2) (2005) 229–237.

[13] N. Sathiparan, U. Rumeshkumar, Effect of moisture condition on mechanical behavior of low strength brick masonry, J. Build. Eng. 17 (2018) 23–31.

[14] S. Sahu, P.R.R. Teja, P. Sarkar, R. Davis, Effect of brick prewetting on masonry bond strength, J. Mater. Civ. Eng. 31 (10) (2019) 06019009.

[15] Standard, I. (1987). Code of practice for structural use of unreinforced masonry. Bureau of Indian Standards, New Delhi.

[16] ASCE 31–03, Seismic evaluation of existing buildings, American Society of Civil Engineers, Reston, 2003.

[17] Leszek Małyszko, Edyta Kowalska, Piotr Bilko, Splitting tensile behavior of autoclaved aerated concrete: comparison of different specimens' results, Constr. Build. Mater. 157 (2017) 1190–1198.

[18] D. Ferretti, E. Michelini, G. Rosati, Cracking in autoclaved aerated concrete: experimental investigation and XFEM modeling, Cem. Concr. Res. 67 (2015) 156–167.

[19] D. Ferretti, E. Michelini, G. Rosati, Mechanical characterization of autoclaved aerated concrete masonry subjected to in-plane loading: experimental investigation and FE modeling, Constr. Build. Mater. 98 (2015) 353–365.

[20] A. Rosti, A. Penna, M. Rota, G. Magenes, In-plane cyclic response of low-density AAC URM walls, Mater. Struct. 49 (11) (2016) 4785–4798.

[21] A.B.E.D. Farid, A. AIDAN, T. IBRAHIM, N. HEGAZI, A.D. Saif, Preparation of a new AAC-concrete sandwich block and its compressive behavior at quasi-static loading, Eng. Trans. 65 (2) (2017) 371–389.

[22] Y. Chen, M. Peng, Y. Zhang, Y. Liu, Mechanical properties of autoclaved aerated concrete with different densities, Adv. Civ. Eng. Mater. 2 (1) (2013) 441–456.

[23] N.R. Devi, P.K. Dhir, P. Sarkar, Influence of strain rate on the mechanical properties of autoclaved aerated concrete, J. Build. Eng. 57 (2022) 104830.

[24] H. Hao, B.G. Tarasov, Experimental study of dynamic material properties of clay brick and mortar at different strain rates, Aust. J. Struct. Eng. 8 (2) (2008) 117–132.

[25] K.N. Feng, D. Ruan, Z. Pan, F. Collins, Y. Bai, C.M. Wang, W.H. Duan, Mechanical behavior of geopolymer concrete subjected to high strain rate compressive loadings, Mater. Struct. 48 (2015) 671–681.

[26] M. Khandelwal, P.G. Ranjith, Z. Pan, J.G. Sanjayan, Effect of strain rate on strength properties of low-calcium fly-ash-based geopolymer mortar under dry condition, Arab. J. Geosci. 6 (2013) 2383–2389.
[27] J.M.L. Reis, A.R. Carvalho, H.S. da Costa Mattos, Effects of displacement rate and temperature on the fracture properties of polymer mortars, Constr. Build. Mater. 55 (2014) 1–4.
[28] J.F. Wang, Y.R. Chen, X.L. Fan, J.Z. Li, Effects of strain rate and confining pressure on compressive behavior of cement asphalt mortar, Mater. Des. 65 (2015) 772–779.
[29] P.G. Ranjith, D. Jasinge, J.Y. Song, S.K. Choi, A study of the effect of displacement rate and moisture content on the mechanical properties of concrete: use of acoustic emission, Mech. Mater. 40 (6) (2008) 453–469.
[30] S. Tandon, K.T. Faber, Effects of loading rate on the fracture of cementitious materials, Cem. Concr. Res. 29 (3) (1999) 397–406.
[31] B.H. Oh, Fracture behavior of concrete under high rates of loading, Eng. Fract. Mech. 35 (1-3) (1990) 327–332.
[32] R. Jasiński, Ł. Drobiec, Comparison research of bed joints construction and bed joints reinforcement on shear parameters of AAC masonry walls, J. Civ. Eng. Archit. 10 (12) (2016) 1329–1343.
[33] Mallikarjuna, S. (2017). Experimental determination of parameters for a micro-modeling-based failure criterion for AAC block masonry shear wall. MTech thesis, Indian Institute of Technology, Guwahati, India.
[34] A. Bhosale, N.P. Zade, P. Sarkar, R. Davis, Mechanical and physical properties of cellular lightweight concrete block masonry, Constr. Build. Mater. 248 (2020) 118621.
[35] A. Raj, A.C. Borsaikia, U.S. Dixit, Compressive and shear bond strengths of grooved AAC blocks and masonry, Mater. Struct. 52 (6) (2019) 1–15.
[36] A. Raj, A.C. Borsaikia, U.S. Dixit, Bond strength of Autoclaved Aerated Concrete (AAC) masonry using various joint materials, J. Build. Eng. 28 (2020) 101039.
[37] N. Mojsilović, M. Petrović, X.R. Anglada, Masonry elements with multi-layer bed joints: behaviour under monotonic and static-cyclic shear, Constr. Build. Mater. 100 (2015) 149–162.
[38] S. Barattucci, V. Sarhosis, A.W. Bruno, A.M. D'Altri, S. de Miranda, G. Castellazzi, An experimental and numerical study on masonry triplets subjected to monotonic and cyclic shear loadings, Constr. Build. Mater. 254 (2020) 119313.
[39] H. Hernoune, B. Benabed, R. Abousnina, A. Alajmi, A.M.G. Alfadhili, A. Shalwan, Experimental research and numerical analysis of CFRP retrofitted masonry triplets under shear loading, Polymers 14 (18) (2022) 3707.
[40] A.M. D'Altri, V. Sarhosis, G. Milani, J. Rots, S. Cattari, S. Lagomarsino, S. de Miranda, Modeling strategies for the computational analysis of unreinforced masonry structures: review and classification, Arch. Comput. Methods Eng. 27 (2020) 1153–1185.
[41] D. Ferretti, E. Michelini, G. Rosati, Cracking in autoclaved aerated concrete: experimental investigation and XFEM modeling, Cem. Concr. Res. 67 (2015) 156–167.
[42] P.B. Lourénço, R. De Borst, J.G. Rots, A plane stress softening plasticity model for orthotropic materials, Int. J. Numer. Methods Eng. 40 (21) (1997) 4033–4057.
[43] P.B. Lourenço, J.G. Rots, J. Blaauwendraad, Continuum model for masonry: parameter estimation and validation, J. Struct. Eng. 124 (6) (1998) 642–652.
[44] ASTM C1693–11 (2017). Standard specification for autoclaved aerated concrete (AAC). American Society for Testing and Materials, west Conshohocken, PA.
[45] ASTM C1161–18 (2018). Standard test method for flexural strength of advanced ceramics at ambient temperature. American Society for Testing and Materials, West Conshohocken, PA.
[46] L. Jin, W. Yu, X. Du, Size effect on static splitting tensile strength of concrete: experimental and numerical studies, J. Mater. Civ. Eng. 32 (10) (2020) 04020308.
[47] M. Moniruzzaman, F. Du, N. Romero, K.I. Winey, Increased flexural modulus and strength in SWNT/epoxy composites by a new fabrication method, Polymer 47 (1) (2006) 293–298.
[48] F. Mujika, On the difference between flexural moduli obtained by three-point and four-point bending tests, Polym. Test. 25 (2) (2006) 214–220.
[49] ASTM C109/C109M-20b (2020). Standard Test Method for Compressive Strength of Hydraulic Cement Mortars (Using 2-in. or [50 mm] Cube Specimens). American Society for Testing and Materials, West Conshohocken, PA.
[50] ASTM C348–21 (2021). Standard test method for flexural strength of hydraulic-cement mortars. American Society for Testing and Materials, West Conshohocken, PA.
[51] BIS (Bureau Indian Standards). 1987.Code of practice for structural use ofunreinforced masonry. IS 1905. New Delhi, India: BIS.
[52] ANSI, American National Standard specifications for modified dry-set cement mortar (American National Standard Institute). ANSI A118.4, ANSI, New York, 2012.
[53] Syst`emes D., Abaqus, R.I.: Dassault Syst`emes, 2022. ⟨http://www.3ds.com/products-services/simulia/products/abaqus/⟩.
[54] J. Lee, G.L. Fenves, A plastic-damage concrete model for earthquake analysis of dams, Earthq. Eng. Struct. Dyn. 27 (9) (1998) 937–956.
[55] B.D. Scott, R. Park, M.J. Priestley, Stress-strain behavior of concrete confined by overlapping hoops at low and high strain rates (January), J. Proc. Vol. 79 (No. 1) (1982) 13–27.
[56] P.J.B.B. Lourenço, Computational strategies for masonry structures, Delft University of Technology, Holland, 1997 (Doctoral dissertation).
[57] P.K. Dhir, E. Tubaldi, A. Orfeo, H. Ahmadi, Cyclic shear behaviour of masonry triplets with rubber joints, Constr. Build. Mater. 351 (2022) 128356.